

A COMPARISON OF BEAMFORMING ALGORITHMS FOR 3D ULTRASOUND IMAGING IN AIR

Marco Moebus and Abdelhak Zoubir

Signal Processing Group
Institute of Telecommunications
Technische Universität Darmstadt
Merckstr. 25, 64283 Darmstadt, Germany
{moebus,zoubir}@ieee.org

ABSTRACT

In acoustic imaging systems, it is crucial to distinguish artifacts from real objects in images obtained from a scene of interest in order to segment and classify obstacles, say for a reverse parking car. In this application, subspace methods are not applicable because of the spatial spread of the objects. This paper analyzes the performance of several beamforming algorithms. We assess the behavior of the algorithms based on real data measurements and measure the performance using a similarity index and power distribution.

Index Terms— acoustic imaging, beamforming, array signal processing, autonomous navigation

1. INTRODUCTION

Acoustic imaging has been successfully used in such different fields as sonar, medical imaging and material testing. In order to create images of a scene of interest, one has to record scattering signals either using a lens system or an array of acoustic sensors (see e.g. [1]). While most applications of acoustic imaging systems operate in media such as dense materials (human tissue, water or metal), systems working in air can be employed in applications such as autonomous navigation and scene reconstruction for example for object detection and classification in a reverse parking scenario, pedestrian detection for active safety systems, to mention a few.

In array systems, signal processing crucially determines the nature of the created images and thereafter the overall system performance. Albeit the existence of high-resolution subspace algorithms, these methods can not be applied in situations where the objects have a non-negligible spatial spread. This is due to the fact that the sources cannot be modeled as point sources and therefore, eigenvalues do not match single sources. Although some work has been done to extend these methods to spatially spread sources for

Direction-Of-Arrival (DOA) estimation, the focus is merely on an increase of estimation accuracy [2].

It is not possible to apply these extensions to source *imaging*. Hence, acoustic imaging systems that have no prior knowledge about the objects to be imaged have to use beamforming algorithms to create the spatial spectrum. In this paper, the effect of different beamforming algorithms is analyzed in the context of acoustic imaging systems that employ ultrasound in air.

We investigate the effects of different beamforming algorithms on the created images of the scene and compare these images in terms of artifacts and object visibility. A presentation of the used imaging system is given in Section 3, followed by the description of quality criteria and the used figures of merit in Section 4. A similarity index is described which allows to evaluate the performance of the algorithms based on experiments described in Section 5. Finally, results are discussed and conclusions drawn.

3. THE IMAGING SYSTEM

We recently presented an acoustic imaging system that uses a single ultrasound transmitter and a 2D receiver array to generate 3D images of the region of interest in a scene of a mobile system [3]. The scene to be analyzed is illuminated by the transmitter, emitting a short narrow-band acoustic pulse with center-frequency $f_c = 50\text{kHz}$. This pulse is reflected by objects present in the scene and backscattering is recorded by the 2D array. Echoes are identified and a spatial spectrum image is generated for each echo segment. Based on a Time-Of-Flight (TOF) estimation, the images can be translated into a 3D map (see Figure 1).

As the system has to operate in an *a priori* unknown environment, subspace-based methods cannot be employed. Therefore, a 2D Capon beamformer was used to scan a two-dimensional grid in the (θ, ϕ) -space (see e.g. [5]). The intensity of a pixel in the images is therefore proportional to the power at each point in this grid.

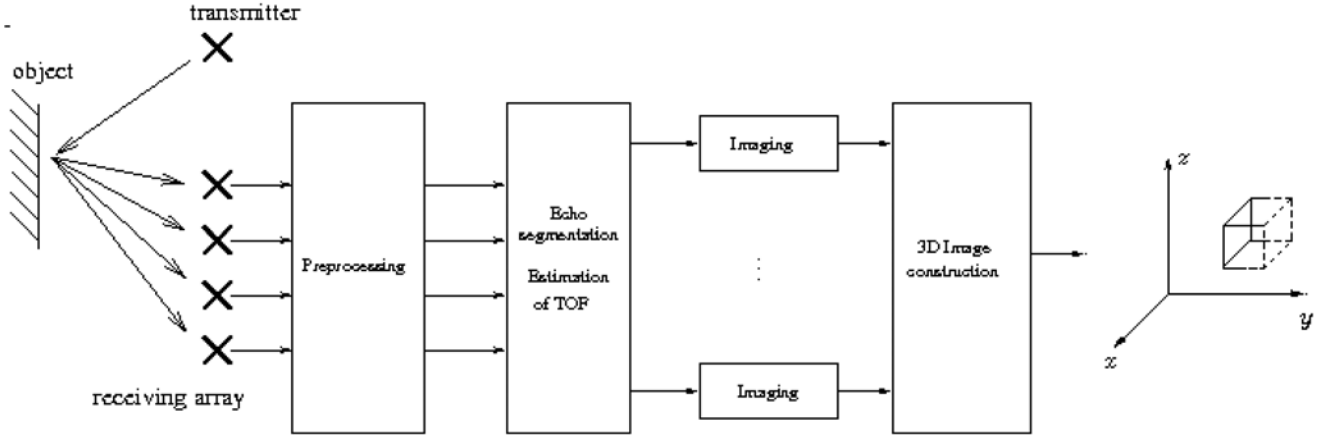


Figure 1: Flowchart of the imaging system

4. QUALITY CRITERIA & THE SSIM

The images we obtain by the system described above form the basis for object detection and classification. It is therefore crucial to create images which represent the physical scene in a way that allows for clear discrimination of objects from artifacts. More specifically, the beam pattern should not allow for artefacts due to sidelobes while the reflections of the objects should be represented distinctively. As the strength of ultrasound echoes varies greatly with range, shape and surface of the objects, any variations of sensitivity in the beam patterns over the whole search space are undesirable. While these criteria are conflicting, the question remains how the beamforming algorithms fulfill those and what differences are present in the resulting images.

We compare the beamforming algorithms by the Structured Similarity Index (SSIM) [4]. It is a similarity measure which was introduced in the image processing community as a means of comparing images based on structural information. Additionally to the single quantity of the index, a map showing local similarities between two images can be calculated. Similarity is measured by statistics based on luminance and contrast. As a third component, the structural information of the images is compared by measure similar to the correlation coefficient, based on pivoted statistics for luminance and contrast.

The index provides both global and local information about the similarity of two images. In our application, we compare the obtained, normalized images to a perfect binary reference image. In addition to the SSIM, we also compute the variance of the power distribution in the object region to compare how power is received from a single surface. The average power per pixel present in the non-object region is

measured to determine the overall strength of the artefacts in the images.

5. EXPERIMENTS

The experiments in this section have been conducted in an acoustic laboratory. To exclude effects of the array geometry on the image, all objects have been recorded with a 20x20-element array. All images were processed using a grid resolution of 1° in both dimensions and are displayed in a logarithmic scaling.

5.1 Rough surface structure - Continuous response

In this experiment, a circular pole with diameter $d = 0.185$ m was placed in front of the array. The surface of the object shows a rough structure in the dimension of λ , such that the scattering on its surface is highly affected. As can be seen in Figures 2 and 3, the created images show a continuous response over the whole surface, independent of the used beamformer. However, the exact distribution of power seen by the array is determined by the beam pattern and therefore the used beamforming algorithm. Artifacts in the images mainly depend on the side lobe structure of the beam pattern. In Figure 2, Capon's beamformer received a very constant power level from the whole surface of the pole which fronts the array. Due to its adaptive character, side lobe effects are minimized such that the object is clearly visible whereas the rest of the images only contain artifacts that are more than 10dB weaker. For the same object Bartlett's beamformer [5] shows peaks on the same region, but the response is not as constant as for Capon's beamformer. There are clearly two peaks visible at both ends of the pole along the θ -dimension.

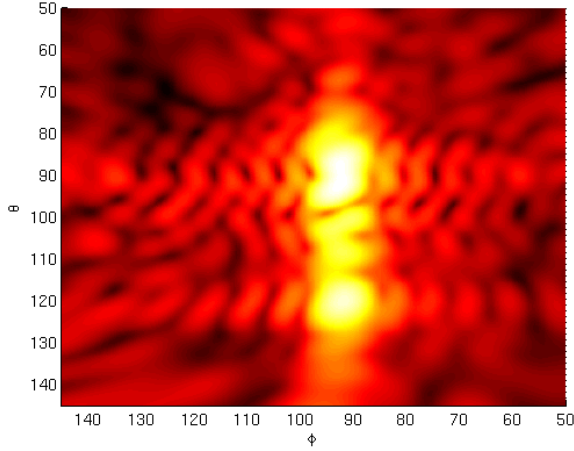


Figure 2: Image of a rough surface object obtained with Bartlett's beamformer.

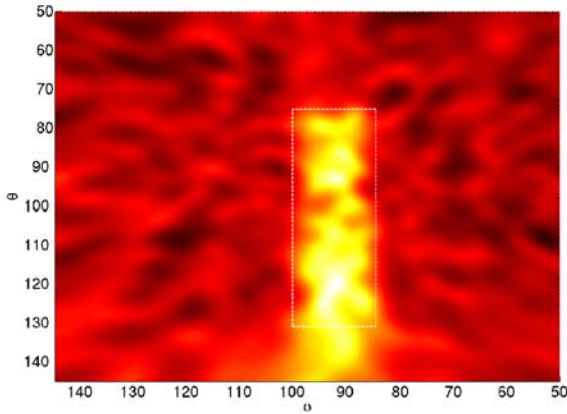


Figure 3: Image of a rough surface object obtained with Capon's beamformer.

The above results can be explained by the peak side lobe of the non-adaptive beam pattern of the algorithm. The side lobe effect is also more clearly visible than for Capon's beamformer in non-object regions. Artifacts are stronger because a larger amount of power reflected from the object is captured by side lobes when looking in regions where no object is actually present.

In Table 1, the effects in the images are summarized. While the SSIM index is on the same level in the object region

($SSIM_O$) for both algorithms, Bartlett's beamformer performs worse in the non-object region ($SSIM_{NO}$). Average power per pixel in the object region (σ_O^2) is slightly less for Capon's beamformer than for Bartlett's, whereas the variance of power is significantly less in that region ($\tilde{\sigma}_O^2$). However, comparing overall power in the non-object region (σ_{NO}^2), the Bartlett beamformer performs much better.

	$SSIM_O$	$SSIM_{NO}$	σ_O^2	$\tilde{\sigma}_O^2$	σ_{NO}^2
Bartlett	0.8886	0.0268	0.1987	$1.3e^{-7}$	0.0460
Capon	0.8852	0.0331	0.1773	$9.3e^{-16}$	0.1247

Table 1: Performance for continuous response.

5.2 Smooth Surface – Specular Response

We recorded data from another object with the same shape, but a smooth surface. This leads to a highly specular scattering at the object and therefore much lower peak amplitude in echoes. Additionally, echoes are received only from spots on the object. In such scenarios, the discrimination between artifacts and object echoes is much more difficult. As can be seen in Figures 3 and 4, the object is not visible by its whole surface anymore. Only a direct reflection, ground reflection and a reflection from the upper edge are visible. However, this is much better in the image based on Capon's beamformer, as the side lobe effects are stronger than in the previous experiment. Considering the overall spatial spread from which energy is received is much smaller, it seems that Bartlett's beamformer is incapable of sharply discriminating objects from background. As shown in Table 2, the SSIM is similar to the results from the previous experiment. However, due to the specular scattering, sharper peaks occur in the images and the average power per pixel is

	$SSIM_O$	$SSIM_{NO}$	σ_O^2	$\tilde{\sigma}_O^2$	σ_{NO}^2
Bartlett	0.8768	0.0371	0.0040	$1.7e^{-6}$	0.0015
Capon	0.8740	0.0425	0.0193	$4.2e^{-12}$	0.00079

Table 2: Performance for specular response.

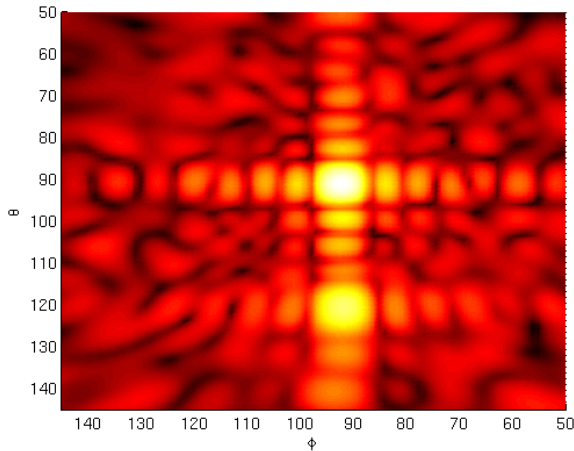


Figure 3: Image of a smooth surface object obtained with Bartlett's beamformer.

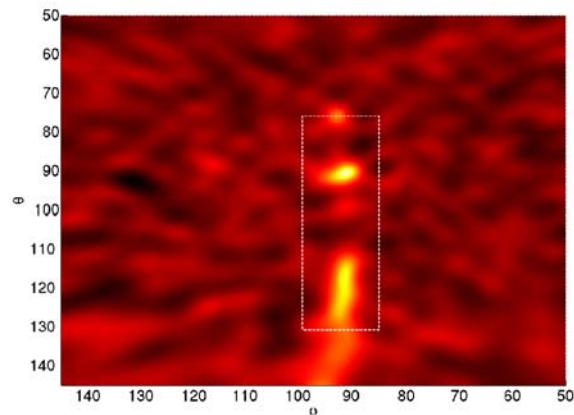


Figure 4: Image of a smooth surface object obtained with Capon's beamformer.

significantly smaller. The main difference is that Capon's beamformer outperforms Bartlett's even when considering power in the non-object region. Additionally, one can see that Capon's beamformer clearly shows the upper edge of the object and also shows narrower peaks in general. The ground reflection aligned along the symmetry axis is clearly identifiable.

6. CONCLUSION

The created images show that Bartlett's beamformer suffers from high side lobe effects that degrade the image quality and visibility of the object in both types of typical echo scattering scenes, whereas Capon's beamformer remains an almost constant power receptor over the surface of the whole objects for continuous scattering. For specular

responses, Bartlett's beamformer is not able to separate the object from the background very well and shows, due to its wider main lobe, generally broader peaks.

REFERENCES

- [1] V. Murino, A. Trucco, "Three-dimensional image generation and processing in underwater acoustic vision", Proceedings of the IEEE, vol. 88, no. 12, pp. 1903--1948, 2000.
- [2] M. Tapio, "Direction and spread estimation of spatially distributed signals via the power azimuth spectrum", Proceedings of the IEEE International Conference on Acoustics, Speech, and Signal Processing (ICASSP '02), Orlando, USA, 2002.
- [3] M. Moebus, A.M. Zoubir, "Three-Dimensional ultrasound imaging in air using a 2D array on a fixed platform", Proceedings of the IEEE International Conference on Acoustics, Speech, and Signal Processing (ICASSP '07), Honolulu, USA, 2007.
- [4] Zhou Wang, A.C. Bovik, H.R. Sheikh, and E.P. Simoncelli, "Image quality assessment: from error visibility to structural similarity", IEEE Transactions on Image Processing, vol. 13, no. 4, pp. 600--612, 2004.
- [5] H. Krim and M. Viberg, "Two decades of array signal processing", IEEE Signal Processing Magazine, vol. 13, no. 4, pp. 67-94, 1996.